HETEROGENEOUS OXYGEN ISOTOPIC COMPOSITION OF A COMPLEX WARK-LOVERING RIM AND THE MARGIN OF A REFRACTORY INCLUSION FROM LEOVILLE. J. I. Simon[1], J. E. P. Matzel[2], S. B. Simon[3], P. K. Weber[2], L. Grossman[3], D. K. Ross[1,4], and I. D. Hutcheon[2]. [1]Center for Isotope Cosmochemistry and Geochronology, ARES NASA-JSC, Houston, TX 77058, USA (Justin.I.Simon@NASA.gov), [2]LLNL, Livermore, CA 94551, USA, [3]The University of Chicago, Chicago, IL 60637, USA, [4]Jacobs Tech., TX 77058, USA.

Introduction: Wark-Lovering (WL) rims [1] surrounding many refractory inclusions represent marker events in the early evolution of the Solar System in which many inclusions were exposed to changes in pressure [2], temperature [3], and isotopic reservoirs [4-7]. The effects of these events can be complex, not only producing mineralogical variability of WL rims [2], but also leading to mineralogical [8-10] and isotopic [7, 11, 12] changes within inclusion interiors. Extreme oxygen isotopic heterogeneity measured in CAIs has been explained by mixing between distinct oxygen gas reservoirs in the nebula [13]. Some WL rims contain relatively simple mineral layering and/or are isotopically homogeneous [14, 15]. As part of a larger effort to document and understand the modifications observed in some CAIs, an inclusion (L6) with a complex WL rim from Leoville, a member of the reduced *CV3* subgroup was studied. Initial study of the textures and mineral chemistry was presented by [16]. Here we present NanoSIMS oxygen isotopic measurements to complement these petrologic observations.

Sample: L6 is a pristine compact Type A (CTA) inclusion with clusters of spinel (typically euhedral, ~50 μm across) and fassaite grains (anhedral) enclosed in visually unaltered melilite that exhibits normal compositional zoning ($Åk_{3-30}$) within the margin (~200 μm) of the inclusion [16]. At the edge of the inclusion is a nearly continuous and often thick (up to 100 μm) layer of spinel intergrown with the melilite interior. Outside of the main spinel layer are additional layers composed of pyroxene ±melilite. Based on petrography and mineral chemistry [16], five generations of pyroxene were identified in the WL rim. In the section studied herein, the innermost is Ti-bearing (Ti-pyx) and appears intergrown with the "main" spinel layer. This Ti-pyx (≤10 μm) becomes less Ti-rich outward and is intergrown with a mixed layer of fine-grained melilite and spinel of varying thickness. Locally the fine-grained melilite layer has a range of grain sizes and can be found in contact with the "main" spinel layer. Coarser melilite tends to enclose less spinel. In places, a second Ti-pyx-melilite layer exists with a distinct Ti-pyx composition from the first [16]. Finally, the entire inclusion and complex rim is surrounded by a uniform layer of diopside (~15 μm), in some places in direct contact with Ti-pyx from an inner layer and sometimes directly overlying the irregular fine-grained mixed melilite-spinel layer (Fig. 1).

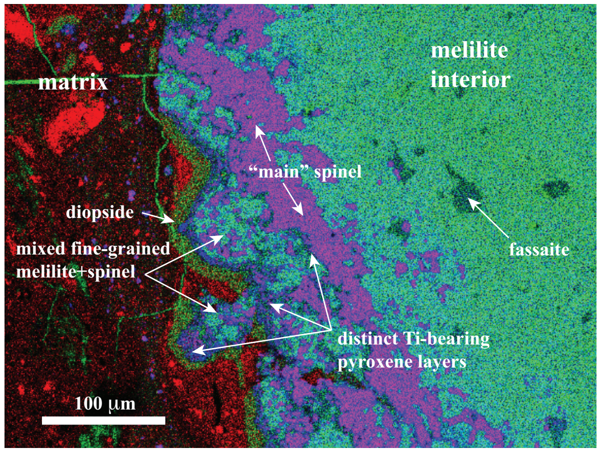

Figure 1. Mg (red), Ca (green), Al (blue) X-ray image of L6 exhibiting a "simple" example of the Wark-Lovering rim stratigraphy surrounding the inclusion.

Methods: We used the LLNL NanoSIMS 50 to perform oxygen isotopic measurements following published methods [7]. Data come from multiple traverses across the rims and outer margin of the interior of L6 to define oxygen isotopic zoning profiles. Data points are ~2 μm diameter single-phase analyses as evaluated by their $^{28}Si/^{16}O$ ion ratios and SEM imagery after the NanoSIMS measurements. Oxygen isotope compositions are reported as $\Delta^{17}O=\delta^{17}O-0.52x\delta^{18}O$, which represents the departure from the terrestrial mass fractionation (TMF) line that defines the terrestrial oxygen reservoir. Based on standard analyses, the precision is <3‰/amu (2σ). We evaluated instrumental mass fractionation (IMF) and reproducibility by repeat analyses of spinel, anorthite, grossular, pyroxene, and forsterite standards. The difference in $\Delta^{17}O$ among the terrestrial standard minerals was similar to our typical uncertainty (~3.0‰). Mineral compositions, and X-ray and backscattered electron maps were used to guide NanoSIMS traverses and verify the mineralogy of analysis spots.

Results: Oxygen isotope data come from traverses spanning the WL rims and/or margin of the interior (Fig. 2). Like several CAIs studied previously [7, 17, 18], L6 exhibits large variations in $\Delta^{17}O$ (>20‰). Compared to the inclusion reported by [7], interior melilite in L6 is more homogeneous and ^{16}O-poor ($\Delta^{17}O$ ~ -6‰). The exception is a systematic $\Delta^{17}O$ decrease from ~ -6‰ to -22‰ at the edge. Spinels in the "main" layer at the margin are ^{16}O-rich ($\Delta^{17}O \leq$ -25‰). The Ti-pyx layers have intermediate $\Delta^{17}O$ compositions ($\Delta^{17}O$ ~ -14 to -18‰). Melilite from the mixed layer exhibits extreme oxygen isotopic heterogeneity with $\Delta^{17}O$ values ranging from ~ -6‰, like a majority of the interior crystals, to -27‰ in one melilite. Diopside in the outermost layer exhibits less variability with $\Delta^{17}O$ from -15‰ to -23‰.

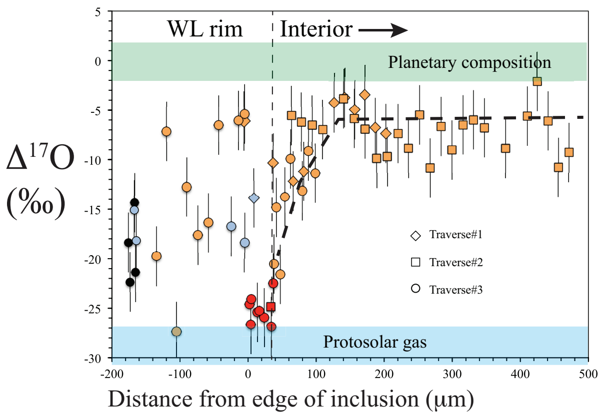

Figure 2. Oxygen isotopic zoning across the Wark-Lovering rim layers and melilite margin of L6 obtained by NanoSIMS. Individual traverses are identified by symbol; melilite analyses are tan, spinel red, Ti-pyx blue, and diopside black. Thick dashed curve emphasizes the oxygen isotopic zoning in melilite at the margin of L6. Spinel and the most ^{16}O-rich rim melilite match the oxygen isotope composition of [19] and likely represent the protosolar composition.

Discussion: The fine-scale spatial zoning and textural features create concern if the mineral analyses represent pure phases. A quantitative means to evaluate this possibility is shown in Fig. 3 where we plot the $^{28}Si^-/^{16}O^-$ secondary ion ratio versus distance for the data shown in Fig. 2; data are not corrected for differences in ion yield. If the ^{16}O-rich composition of melilite was due to overlap of the primary beam onto spinel, the $^{28}Si^-/^{16}O^-$ ratio would show marked changes from the ~0.02 value consistent with pure melilite.

Oxygen isotope compositions within the interior and compositional zoning at the margin of L6 show great similarity to a previously studied CAI (Ef-1), a CTA from Efremovka [17]. The WL rim on L6 is much more complicated (both mineralogically and isotopically). The oxygen isotopic compositions of the WL rim phases share some similarity to previously studied WL rims [7, 17], e.g., spinel is generally ^{16}O-rich while pyroxene has intermediate $\Delta^{17}O$ values. The wealth of melilite data from a WL rim is new, as is the extreme O-isotope heterogeneity. Three Ti-pyx layers seen in [16] appear to have similar oxygen isotopic compositions to one another, indicating that there were more cycles of deposition than recorded by isotopic differences. The average diopside $\Delta^{17}O$ value is slightly more ^{16}O-rich than the average Ti-pyx value (from any or all inner Ti-pyx layers). Likewise, melilite in the WL-rim exhibits a general inward trend towards ^{16}O-poor values despite the existence of ^{16}O-rich melilite at the edge of the inclusion. Although it is assumed that the inclusion formed from an ^{16}O-rich protosolar gas [19], the general sense of zoning in the WL-rim, as well as the zoning in melilite at the margin of the inclusion, suggest that the inclusion progressively exchanged or formed from ^{16}O-poor and then ^{16}O-rich reservoirs. The heterogeneity within the interior supports our previous conclusion that CAIs record a progressive trend in the extent of exchange with a number of isotopically distinct reservoirs that is decoupled from mineralogical evidence of secondary alteration [17]. The WL rim and interior data support models in which CAIs were transported between at least two distinct nebular gases multiple times, e.g., [7].

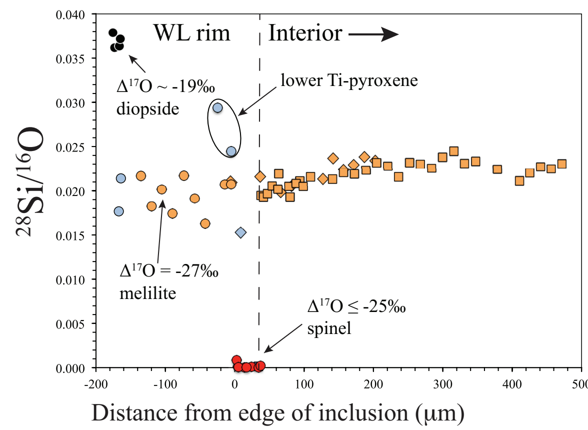

Figure 3. $^{28}Si/^{16}O$ ion ratio profile across the minerals in the Wark-Lovering rim layers and interior of L6 used to identify data that could come from analytical mixtures. Spurious data are not shown (see text). Shifts in $^{28}Si^-/^{16}O^-$ among melilite and between innermost high Ti-pyx, lower Ti-pyx, and diopside, combined with $\Delta^{17}O$ indicate negligible contamination from spinel and are those generally expected from their chemical compositions. Symbols are as in Fig. 2.

References: [1] Wark, D.A. and J.F. Lovering (1977) *PLSC*, 95-112. [2] Simon, J.I. et al. (2005) *EPSL*, 238, 272-283. [3] Young, E.D. et al. (2005) *Science*, 308, 223-227. [4] Yurimoto, H. et al. (1998) *Science*, 282, 1874-1876. [5] Krot, A.N. et al. (2002) *Science*, 295, 1051-1054. [6] Aleon, J. et al. (2007) *EPSL* 263, 114-127. [7] Simon J.I. et al. (2011) *Science*, 2011, 1175-1178. [8] Keller, L.P. and P.R. Buseck (1991) *Science*, 1991, 252, 947-949. [9] Metzler, K., A. et al. (1992) *GCA*, 56, 2873-2897. [10] Jacobsen, B. et al. (2011) *ApJL*, 2011. 731(L28). [11] Fagan, T.J. et al. (2004) *MPS*, 39, 1257-1272. [12] Simon, J.I. and E.D. Young (2011) *EPSL*, 304, 468-482. [13] Clayton, R.N. et al. (1977) *EPSL*, 34, 209-224. [14] Matzel, J.E.P. et al. (2013) *LPSC* Abst. #2632. [15] Bodénan, J.-D. et al. (2013) *Metsoc* Abst. #5187. [16] Simon, S.B. and L. Grossman (2013) *LPSC* Abst. #2793. [17] Simon, J.I. et al. (2012) *LPSC* Abst. #1340. [18] Simon, J.I. et al. (2013) *LPSC* Abst. #1828. [19] McKeegan, K.D. et al. (2011) *Science*, 332, 1528-1532.